SFB/CPP-11-40
TTP11-21

Production of scalar and pseudo-scalar Higgs bosons to next-to-next-to-leading order at hadron colliders

Alexey Pak, Mikhail Rogal, Matthias Steinhauser

Institut für Theoretische Teilchenphysik
Karlsruhe Institute of Technology (KIT)
76128 Karlsruhe, Germany

Abstract

We consider the production of intermediate-mass CP-even and CP-odd Higgs bosons in proton-proton and proton-anti-proton collisions. We extend the recently published results for the complete next-to-next-to-leading order calculation for a scalar Higgs boson to the pseudo-scalar case and present details of the calculation that might be useful for similar future investigations. The result is based on an expansion in the limit of a heavy top quark mass and a subsequent matching to the expression obtained in the limit of infinite energy. For a Higgs boson mass of 120 GeV the deviation from the infinite-top quark mass result is small. For 300 GeV, however, the next-to-next-to-leading order corrections for a scalar Higgs boson exceed the effective-theory result by about 9% which increases to 22% in the pseudo-scalar case. Thus in this mass range the effect on the total cross section amounts to about 2% and 6%, respectively, which may be relevant in future precision studies.

PACS numbers: 12.38.Bx 14.80.Bn 14.80.Cp

1 Introduction

One of the most urgent problems in the modern particle physics is unveiling the origin of masses of elementary particles, which according to the Standard Model (SM) is closely related to the Higgs boson. A lower limit on the Higgs boson mass of about 114 GeV was set more than ten years ago by the experiments on the Large Electron-Positron Collider (LEP) [1] and more recently mass values around 160 GeV were excluded by the `Tevatron` [2].[1] Due to rarity of the process, discovering the Higgs boson production requires subtle experimental methods and precise theoretical predictions.

The Standard Model contains only one physical CP-even Higgs boson. However, many extensions of the SM, such as two-Higgs-doublet models or supersymmetric models predict also charged and CP-odd Higgs bosons. In this paper we consider the production of a pseudo-scalar Higgs boson in the form of an external current with a generic Yukawa coupling. We require that the coupling be proportional to the heavy quark mass, while the coefficient can be specified within any desired model.

The dominance of the gluon-fusion process in the production of a scalar or a pseudo-scalar Higgs boson was established in the end of the 1970's [4–7]. Later, in the beginning of the 1990's, several groups obtained the next-to-leading order (NLO) QCD corrections [8–10]. The latter appeared to be large, modifying the LO prediction by as much as 100%. Thus, the accurate prediction necessitated the next-to-next-to-leading order (NNLO) calculation.

The NLO results include the complete dependence on the partonic center-of-mass energy ($\hat{s}$), the Higgs boson mass (M_Φ) and the top quark mass (M_t) [10, 11]. Assuming an infinitely heavy top quark, one considerably simplifies the calculation while introducing only a few per cent error. The NNLO corrections were first computed in this limit, for the scalar Higgs boson in Refs. [12–15] and for the pseudo-scalar in Refs. [15–17]. More recently, the missing top mass-suppressed corrections to the scalar Higgs production were estimated and found small [18–20] compared to other uncertainties. In these papers the mass dependence was recovered by interpolating between the expansion of the cross section near the heavy top limit and the leading asymptotics in the $\hat{s} \to \infty$ limit, given in Ref. [20, 21].

In this paper we apply the technique used in Ref. [19] and provide similar top mass-suppressed corrections to the pseudo-scalar Higgs boson production. We compute five expansion terms of the cross section in $1/M_t^2$, and match the partonic cross sections to the values of Ref. [22], derived in the $\hat{s} \to \infty$ limit.

Similarly to the conclusions of Refs. [18–20], we find that the infinite-top quark mass approximation with factorized exact LO mass dependence receives relatively small corrections. We are not aware of any trivial explanations of this behaviour. Note that assuming no factorization of the exact LO quark mass dependence the $1/M_t^0$ result au-

[1] We refer to [3] for critical comments on the `Tevatron` analysis.

gumented with $\hat{s} \to \infty$ behaviour deviates far from the infinite-top mass result, and only after including at least the $1/M_t^6$ corrections the agreement of hadronic cross sections reaches the level of a few percent.

For completeness let us also mention several results that improve upon the fixed-order QCD. Those include the soft-gluon resummation to next-to-next-to-leading [23] and next-to-next-to-next-to-leading [24–26] logarithmic orders and the identification (and resummation) of certain π^2 terms [27] that significantly improves the convergence of the perturbative series. Recent numerical predictions of Higgs boson production in gluon fusion both at the Tevatron and the LHC are summarized in Ref. [28–30]. For reviews, see Refs. [31, 32].

The remainder of the paper is organized as follows: in the next Section we introduce our notation and the basic formalism. After that, we describe the treatment of γ_5 for the case of the pseudo-scalar Higgs boson. In Section 3 we concentrate on the NLO prediction and compare our approximations to the exact result both at the partonic and the hadronic levels. Section 4 is devoted to the NNLO partonic corrections and Section 5 discusses the hadronic cross section. Results are presented for the `LHC` running at 14 TeV center-of-mass energies. Conclusions are presented in Section 6. In Appendix A we discuss the phase space master integrals expanded to the ϵ order sufficient for a N^{3}LO calculation. Technical details of the convolutions of various functions are given in Appendix B.

2 Preliminaries

2.1 Notation and the LO result

In the full theory, the scalar and the pseudo-scalar Higgs bosons couple to fermions via the following terms in the Yukawa Lagrange density:

$$\mathcal{L}_Y = -g_q^{Y,H} m_q^0 \frac{H^0}{v^0} \bar{q}^0 q^0 - g_q^{Y,A} m_q^0 \frac{A^0}{v^0} \bar{q}^0 i\gamma^5 q^0 \,, \tag{1}$$

where the dimensionless couplings $g_q^{Y,H}$ and $g_q^{Y,A}$ specify the coupling strength of the Higgs bosons to the heavy quark q. The cross section of the pseudo-scalar Higgs boson production is proportional to $(g_q^{Y,A})^2$; in the following discussion of this cross section we drop this constant for convenience.

In the Standard Model $g_q^{Y,H} = 1$, $g_q^{Y,A} = 0$, but in the MSSM, e.g., one has $g_t^{Y,H} \sim 1/\sin\beta$, $g_b^{Y,H} \sim 1/\cos\beta$, $g_t^{Y,A} \sim 1/\tan\beta$, $g_b^{Y,A} \sim \tan\beta$ where $\tan\beta$ is the ratio of the Higgs field vacuum expectation values. Thus, the Higgs coupling to the top quark mass is suppressed for large $\tan\beta$ and our analysis is only valid for small values; for larger values also the contribution from bottom quarks has to be considered (see, e.g., the recent publications [33, 34]).

The superscript “0” in Eq. (1) indicates bare quantities. Since we only consider QCD corrections, there are no counterterms for v^0, H^0 and A^0, and the Higgs field vacuum expectation value is $v = 2^{-1/4} G_F^{-1/2}$. We also introduce the variables

$$\rho = \frac{M_\Phi^2}{M_t^2}\,, \quad x = \frac{M_\Phi^2}{\hat{s}}\,, \tag{2}$$

where $\hat{s}$ is the partonic center-of-mass energy, Φ denotes either scalar (H) or pseudo-scalar (A) Higgs boson and M_t is the top quark pole mass. The divergences in the loop integrals are regularized using dimensional regularization with $d = 4 - 2\epsilon$ space-time dimensions.

The partonic cross section is commonly factorized as

$$\hat{\sigma}_{ij\to\Phi+X}(x) = \hat{A}_{\rm LO}^{\Phi}\left(\delta(1-x) + \left(\frac{\alpha_s}{\pi}\right)\Delta_{ij}^{\Phi,(1)} + \left(\frac{\alpha_s}{\pi}\right)^2\Delta_{ij}^{\Phi,(2)} + \ldots\right), \tag{3}$$

where the factor $\hat{A}_{\rm LO}^{\Phi}$ contains the constants and the complete non-trivial LO ρ-dependence. Such factorization provides an excellent agreement between the exact and the approximated results for the hadronic cross section at the NLO and the NNLO [18–20]. The well-known LO result is

$$\hat{A}_{\rm LO}^{\Phi} = \frac{G_F\,\alpha_s^2}{288\sqrt{2}\pi} f_0^{\Phi}(\rho)\,, \tag{4}$$

with

$$f_0^H(\rho) = \begin{cases} \frac{36}{\rho^2}\left[1 + \left(1-\frac{4}{\rho}\right)\arcsin^2\left(\frac{\sqrt{\rho}}{2}\right)\right]^2, & (\rho \le 4)\,, \\ \frac{9}{4\rho^2}\left|4 - (1-\frac{4}{\rho})\left[\ln\frac{1+\sqrt{1-4/\rho}}{1-\sqrt{1-4/\rho}} - i\pi\right]^2\right|^2, & (\rho > 4)\,, \end{cases} \tag{5}$$

$$f_0^A(\rho) = \begin{cases} \frac{36}{\rho^2}\arcsin^4\left(\frac{\sqrt{\rho}}{2}\right), & (\rho \le 4)\,, \\ \frac{9}{4\rho^2}\left|\ln\frac{1+\sqrt{1-4/\rho}}{1-\sqrt{1-4/\rho}} - i\pi\right|^4, & (\rho > 4)\,. \end{cases} \tag{6}$$

In what follows, whenever we refer to the infinite-top quark mass result we assume the factorization of the exact LO mass dependence as given in Eq. (3).

2.2 Optical theorem and asymptotic expansion

Already at the NLO one has to consider real and virtual contributions which individually contain quadratic poles in ϵ. In our approach we consider the forward scattering amplitude and use the optical theorem in order to derive the inclusive total cross section for the production of Higgs bosons (only the cuts that cross the Higgs boson line should be considered). At the NLO, the possible initial and final states are $gg \to \Phi + (0 \text{ or } 1 \text{ gluon})$, $qg \to \Phi + q$, and $q\bar{q} \to \Phi + g$. At the NNLO, we in addition have reactions $gg \to \Phi + (gg \text{ or } q\bar{q})$, $qg \to \Phi + qg$, $q\bar{q} \to \Phi + (gg \text{ or } q\bar{q})$, $qq \to \Phi + qq$, and $qq' \to \Phi + qq'$. Here q and q' stand for different massless quark flavours.[2] Sample diagrams of the corresponding

[2]It is understood that the ghosts are always considered together with gluons.

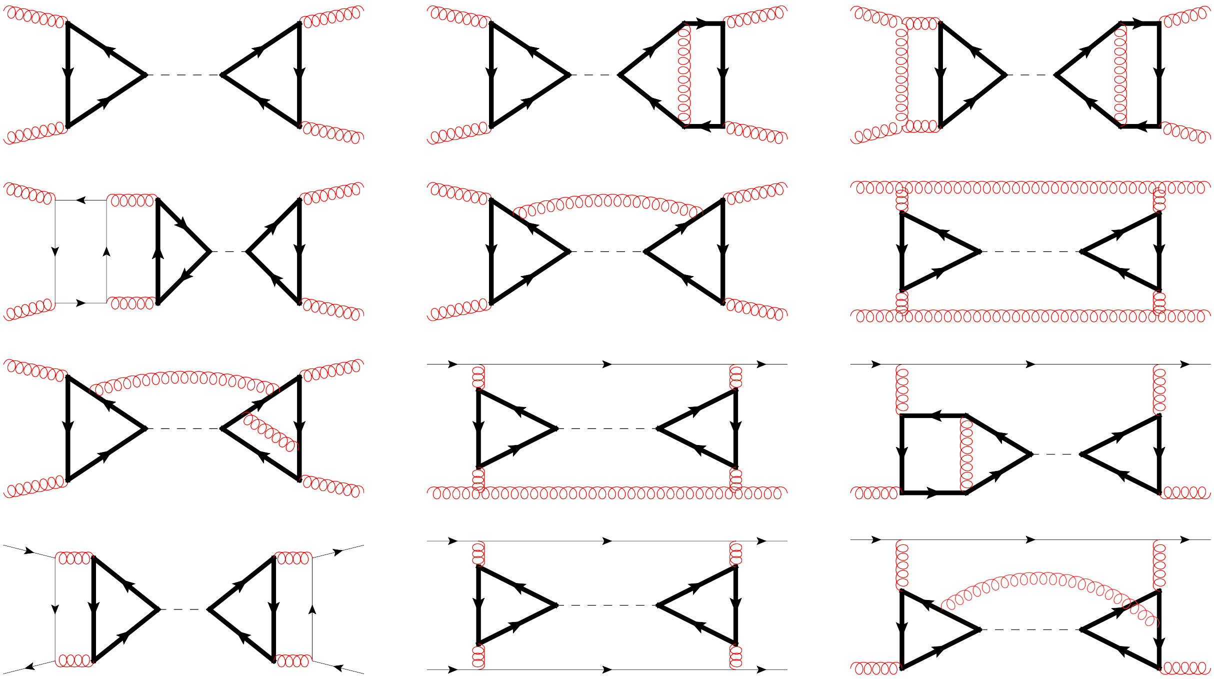

Figure 1: Sample forward scattering diagrams whose cuts correspond to the LO, NLO and NNLO corrections to $gg \to \Phi + gg$, $qg \to \Phi + qg$ and $qq \to \Phi + qq$. Dashed, curly and thick (thin) solid lines represent Higgs bosons, gluons and top (light) quarks, respectively.

forward-scattering amplitudes are shown in Fig. 1.

The expressions are simplified by the forward-scattering kinematics implied by the optical theorem. The proper projectors applied to the external massless particles reduce each amplitude to a scalar expression depending only on ρ and x. Yet, the imaginary part of the double-scale four-loop integral with the exact dependence on both variables is still out of reach with the present methods, and we apply the asymptotic expansion [35] in $\rho \to 0$ which corresponds to the limit $M_t^2 \gg M_\Phi^2, \hat{s}$. After the expansion, every four-loop integral factorizes into one-, two- or three-loop vacuum bubble with the single mass scale M_t, and the tree-level (for the virtual corrections), one- or two-loop box graph depending on x.

The integrals with various denominator exponents that appear during the asymptotic expansion are reduced to a few master integrals using the integration-by-parts (IBP) relations, in which we treat cut lines as normal propagators. The two- and three- particle cuts are again re-introduced in the master integrals and evaluated separately.

In the case of the virtual corrections the imaginary part of the Feynman diagrams arises solely from the factor

$$(-1 + i0)^{a\epsilon} \quad = \quad 1 - i\,(\pi a \epsilon) - \frac{(\pi a \epsilon)^2}{2} + \mathcal{O}(\epsilon^3)\,, \tag{7}$$

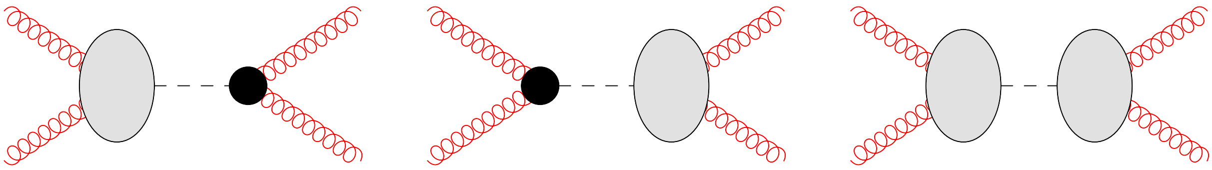

Figure 2: Possible Feynman diagrams for the virtual corrections to the gg-initiated partonic cross section. The shaded blobs represent massless one- or two-loop diagrams, the black dots mark the effective vertices that have no imaginary part.

where in our case $a = 1$ or $a = 2$. Schematically, the occurring diagrams can be divided into three cases sketched for the gg-initiated diagrams in Fig. 2. In the cases (a) and (b) the calculation is straightforward, the loop integrals are evaluated and the factor of Eq. (7) expanded in ϵ. If the grey blob develops an imaginary part, we discard it since it corresponds to a cut outside the Higgs line. The case (c) has massless one-loop integrals on the both sides of the Higgs boson propagator. Here in order to reproduce the corresponding product of a one-loop amplitude and a complex conjugate amplitude, one has to replace the factor $(-1+i0)^{2\epsilon}$ with $(-1+i0)^{\epsilon}(-1-i0)^{\epsilon} = 1$.

2.3 Treatment of γ_5

The optical theorem simplifies the treatment of γ^5 which appears in the coupling of the pseudo-scalar Higgs boson to quarks. We follow the prescription of Ref. [36] for the pseudo-scalar current renormalization, replacing

$$\gamma_5 \to \frac{i}{24}\epsilon_{\mu\nu\rho\sigma}\gamma^{[\mu}\gamma^{\nu}\gamma^{\rho}\gamma^{\sigma]}. \tag{8}$$

The square brackets denote total anti-symmetrization. The 24 terms on the right-hand side of Eq. (8) can be simplified via

$$\frac{1}{24}\gamma^{[\mu}\gamma^{\nu}\gamma^{\rho}\gamma^{\sigma]} = \frac{1}{4}\left(\gamma^{\mu}\gamma^{\nu}\gamma^{\rho}\gamma^{\sigma} + \gamma^{\sigma}\gamma^{\rho}\gamma^{\nu}\gamma^{\mu} - \gamma^{\nu}\gamma^{\rho}\gamma^{\sigma}\gamma^{\mu} - \gamma^{\mu}\gamma^{\sigma}\gamma^{\rho}\gamma^{\nu}\right). \tag{9}$$

Next, one should factor out the ϵ tensor and compute the remaining amplitude in d dimensions. At the very end, when the expressions are finite in the limit $\epsilon \to 0$, one multiplies the result with the ϵ tensor and applies the finite renormalization constant of Ref. [36].

Each forward-scattering amplitude contains two factors of γ_5. After the replacements of Eq. (8) we have the product of two ϵ tensors that can be immediately re-written as the product of four metric tensors with antisymmetrized indices:

$$\epsilon^{\alpha\beta\gamma\delta}\epsilon_{\mu\nu\rho\sigma} = -g_{\mu}^{[\alpha}g_{\nu}^{\beta}g_{\rho}^{\gamma}g_{\sigma}^{\delta]} = -\begin{vmatrix} g_{\mu}^{\alpha} & g_{\mu}^{\beta} & g_{\mu}^{\gamma} & g_{\mu}^{\delta} \\ g_{\nu}^{\alpha} & g_{\nu}^{\beta} & g_{\nu}^{\gamma} & g_{\nu}^{\delta} \\ g_{\rho}^{\alpha} & g_{\rho}^{\beta} & g_{\rho}^{\gamma} & g_{\rho}^{\delta} \\ g_{\sigma}^{\alpha} & g_{\sigma}^{\beta} & g_{\sigma}^{\gamma} & g_{\sigma}^{\delta} \end{vmatrix}. \tag{10}$$

The right-hand side of this equation is defined in d dimensions and can be used during the calculation of the Feynman diagrams which eliminates explicit projectors.

2.4 Alternative approach to virtual corrections

As a cross-check, we evaluated the virtual corrections using two different approaches. First, we use the optical theorem as described above with a simple implementation of γ_5 according to Ref. [36], treating the virtual and the real corrections on the same ground. The finite result is then obtained before applying the finite γ_5 renormalization constant.

In the second method we consider the (pseudo-scalar) Higgs-gluon-gluon vertex diagrams and expand in the (formal) limit $M_t \gg M_H$. This is similar to the calculation of Ref. [37] for the scalar Higgs boson. The amplitudes are multiplied with projectors that couple to Lorentz indices of the gluons and the four additional indices that remain after the epsilon-tensor removal [38].

More explicitly, the pseudo-scalar Higgs-gluon-gluon amplitude has the form

$$A^{\alpha\beta,ab}_{gg\to A} = A^{ab}_{gg\to A}\,\epsilon^{\alpha\beta\mu\nu}q_{1,\mu}q_{2,\nu}\,, \tag{11}$$

where α and a, β and b are the Lorentz and the colour indices of the incoming gluons. After the replacement Eq. (8) $A^{\alpha\beta,ab}_{gg\to A}$ becomes

$$A^{ab}_{gg\to A,\alpha\beta} = \epsilon_{\mu\nu\rho\sigma}A^{\mu\nu\rho\sigma,ab}_{gg\to A,\alpha\beta}\,. \tag{12}$$

Together with Eq. (11) it gives

$$A^{\mu\nu\rho\sigma,ab}_{gg\to A,\alpha\beta} = \frac{1}{24}A^{ab}_{gg\to A}\;q_1^{[\mu}q_2^{\nu}g_\alpha^{\rho}g_\beta^{\sigma]}\,, \tag{13}$$

where q_1 and q_2 are the incoming momenta of the gluons. Now the (Lorentz) scalar amplitude $A^{ab}_{gg\to A}$ can be obtained from $A^{\mu\nu\rho\sigma,ab}_{gg\to A,\alpha\beta}$ via the projector $P^{\alpha\beta}_{\mu\nu\rho\sigma}$ [38]:[3]

$$\begin{aligned} A^{ab}_{gg\to A} &= P^{\alpha\beta}_{\mu\nu\rho\sigma}A^{\mu\nu\rho\sigma,ab}_{gg\to A,\alpha\beta}\,, \\ P^{\alpha\beta}_{\mu\nu\rho\sigma} &= -\frac{q_{1,[\mu}q_{2,\nu}g_\rho^{\alpha}g_{\sigma]}^{\beta}}{(d-2)(d-3)(q_1\cdot q_2)^2}\,. \end{aligned} \tag{14}$$

In the actual calculations we use Eq. (8) in the initial diagram, then drop $\epsilon_{\mu\nu\rho\sigma}$ and obtain $A^{\mu\nu\rho\sigma,ab}_{gg\to A,\alpha\beta}$. Using Eq. (14) and summing the diagrams, we then arrive at $A^{ab}_{gg\to A}$ which has no open Lorentz indices. The virtual contribution to the total cross section is finally obtained by squaring the amplitude Eq. (11) and integrating over the phase space. Accounting for the averaging factors, we find:

$$\hat{\sigma}_{\rm virt} = \frac{\pi}{256}\frac{(d-3)}{(d-2)}\left|A^{ab}_{gg\to A}\right|^2\,. \tag{15}$$

[3] Note that the formulae presented in Ref. [38] apply to the coefficient function of the effective theory whereas here we invesigate the virtual corrections in the full theory.

2.5 Software

To evaluate Feynman diagrams we use the well-tested chain of computer algebra programs developed for the scalar Higgs case [19]. The original diagrams, the corresponding asymptotic expansion prescriptions, and the master integrals are identical to the scalar Higgs case, with only trivial changes. Thus, here we only briefly outline the procedure.

First, the diagrams are generated with `QGRAF` [39] supplemented by additional scripts that eliminate unnecessary graphs. Each diagram is then expanded in the limit $M_t^2 \gg \hat{s}, M_\Phi^2$ using two independent programs: a combination of `q2e` and `exp` [40, 41], and a separate `Perl` program. This turns the original four-loop three-scale integrals into products of single-scale (one-, two-, and three-loop) vacuum bubbles and double-scale forward-scattering integrals (of one and two loops). The latter are reduced to master integrals with our own implementation of the Laporta algorithm [42, 43]. Master integrals have been computed in Ref. [14]; in this calculation we extended them by one order in ϵ which might be useful for the future calculations.

2.6 Initial state singularities

The renormalized sum of the real and the virtual diagrams is not finite in the limit $\epsilon \to 0$. The remaining poles originate from the collinear divergences in the initial state: the initial gluon may split into a quark-antiquark pair, and the quark participate in the Higgs boson production. The corresponding contribution is determined by

$$\begin{aligned} \hat{\sigma}^{\text{renormalized}}_{ij\to\Phi+X}(x) &= \mathcal{R}\left[\hat{\sigma}^{\text{bare}}_{ik} \otimes P_{kj} + P_{ik} \otimes \hat{\sigma}^{\text{bare}}_{kj}\right], \\ P_{ij}(x) &= \delta_{ij}\delta(1-x) + \frac{\alpha_s^{(5),\text{bare}}}{\pi} P^{(1)}_{ij}(x) + \ldots, \end{aligned} \tag{16}$$

where $P^{(k)}_{ij}(x)$ is the splitting function that describes the probability of parton j to emit parton i with the fraction x of its initial energy. $\mathcal{R}$ is the renormalization operation, and $\alpha_s^{(5),\text{bare}}$ is defined as prescribed by the definition of the splitting functions and consistently with the definition of the parton distribution functions (PDFs) which absorb the non-perturbative and non-singular features of the initial state.

In our calculation, we use the common definition consistent with the MSTW08 PDF set, where $\alpha_s^{(5),\text{bare}}$ is the bare coupling in the effective theory with decoupled top quark and $n_f = 5$ massless quarks. The convolution of functions that enter into $P^{(k)}_{ij}(x)$ and $\hat{\sigma}^{\text{bare}}_{kj}$ is defined as

$$[f \otimes g](x) = \int_0^1 \mathrm{d}x_1 \mathrm{d}x_2 \delta(x - x_1 x_2) f(x_1) g(x_2). \tag{17}$$

Appendix B contains the details of evaluation of these integrals. In this context, see also Refs. [14, 15] and references therein.

2.7 From partonic to hadronic cross sections

In order to find the hadronic cross section one has to convolute the partonic cross section with the PDFs which can be written in the form

$$\sigma_{pp\to\Phi+X}(s) \;=\; \sum_{ij}\int_{M_\Phi^2/s}^{1}\mathrm{d}x\left[\frac{\mathrm{d}\mathcal{L}_{ij}}{\mathrm{d}x}\right](x,\mu_F)\;\hat\sigma_{ij\to\Phi+X}(x,\mu_F,\mu_R)\,, \tag{18}$$

where the sum includes all distinct production channels, $ij \in \{gg,\ qg,\ q\bar q,\ qq,\ qq'\}$. The luminosity function $\mathrm{d}\mathcal{L}_{ij}/\mathrm{d}x$ contains the symmetry factors and the convolution of PDFs. For example, the quark-gluon luminosity is given by[4]

$$\begin{aligned}\left[\frac{d\mathcal{L}_{qg}}{\mathrm{d}x}\right](x,\mu_F) \;&=\; 2\sum_{q\in\{u,\ldots,b,\bar u,\ldots,\bar b\}}\int_0^1\mathrm{d}x_1\int_0^1\mathrm{d}x_2\,f_{g/p}(x_1,\mu_F)f_{q/p}(x_2,\mu_F) \\ &\quad\times\delta\left(\frac{M_\Phi^2}{sx}-x_1x_2\right)\frac{M_\Phi^2}{sx^2}\,.\end{aligned} \tag{19}$$

In Ref. [19] the luminosities $\mathrm{d}\mathcal{L}_{ij}/\mathrm{d}x$ have been discussed in some detail; for our purposes it is important to remember that $\mathrm{d}\mathcal{L}_{gg}/\mathrm{d}x$ is practically zero for $x \lesssim 10^{-3}$.

We split the hadronic cross section according to

$$\sigma_{pp'\to\Phi+X}(s) \;=\; \sigma_\Phi^{\mathrm{LO}} + \delta\sigma_\Phi^{\mathrm{NLO}} + \delta\sigma_\Phi^{\mathrm{NNLO}}\,, \tag{20}$$

and add subscript "∞" or "exact" to the quantities in Eq. (20) when referring to the infinite-top quark mass result or the exact expression, respectively. A subscript "n" indicates that corrections through order $1/M_t^n$ have been included. We leave out the subscript Φ in case when the meaning is clear from the context.

We use LO, NLO and NNLO PDFs by the MSTW2008 collaboration [44] in order to obtain the respective predictions for $\sigma_{pp'\to\Phi+X}$ in Eq. (20). The choice of the PDFs determines the values of $\alpha_s(M_Z)\equiv\alpha_s^{(5)}(M_Z)$:

$$\alpha_s^{\mathrm{LO}}(M_Z) \;=\; 0.139384\,,\quad \alpha_s^{\mathrm{NLO}}(M_Z)=0.120176\,,\quad \alpha_s^{\mathrm{NNLO}}(M_Z)=0.117068\,. \tag{21}$$

The appropriate $\overline{\mathrm{MS}}$ beta function then determines $\alpha_s(\mu_R)$ that enters the formulae.

3 NLO cross section

3.1 Partonic cross section

In this subsection we discuss the partonic NLO cross section as a function of $x = M_\Phi^2/\hat s$. As mentioned in the previous section, we computed the partonic cross section in the limit

[4]This definition applies to pp collisions at the `LHC`; its modification for $p\bar p$ collisions at the Tevatron is obvious.

$M_t^2 \gg \hat{s}, M_\Phi^2$. By construction these approximations poorly converge for $\hat{s} > (2M_t)^2$, i.e. in the energy region where top quark pairs can be produced. In terms of the variable x, the threshold is given by $x_{\rm thr} = M_\Phi^2/(4M_t^2)$ which is $x_{\rm thr} = 0.12$ for $M_\Phi = 120$ GeV and $x_{\rm thr} = 0.75$ for $M_\Phi = 300$ GeV. For $x < x_{\rm thr}$ we do not expect our expansion in $1/M_t^2$ to converge.

To cure this problem we follow the suggestions discussed in the literature and match the heavy-top expansion to the leading term in the high-energy expansion obtained in Refs. [20, 21] and [22] for the scalar and pseudo-scalar Higgs boson, respectively. The matching procedure has been successfully applied to the scalar Higgs boson in Refs. [18–20]. In the pseudo-scalar case the matching was done in Ref. [22] based on the leading order approximation in $M_t^2 \gg \hat{s}, M_A^2$. In the following we discuss the effect of the power-suppressed terms and compare to the exact result as implemented in `HIGLU` [45].

Before we discuss our results in detail, let us describe our matching procedure. The expansion near the heavy top limit of the quantities $\Delta_{ij}(x)$ in Eq. (3) has the form[5]

$$\Delta_{ij}^{\rm exp}(x) = \Delta_{ij,0}(x) + \rho\Delta_{ij,1}(x) + \rho^2\Delta_{ij,2}(x) + \dots \tag{22}$$

and is expected to converge for $x > x_{\rm thr}$.

The $x \to 0$ limit of the NLO partonic cross section has the form

$$\Delta_{ij}(x) \stackrel{x\to 0}{=} C_{ij} + \mathcal{O}(x)\,, \tag{23}$$

with coefficients C_{ij} computed in Refs. [20–22]. In order to combine these results we find some matching value $x_m \sim x_{\rm thr}$ and coefficient D_{ij}, so that $\Delta_{ij}(x) = C_{ij} + D_{ij}x$, $x < x_m$, and $\Delta_{ij}(x) = \Delta_{ij}^{\rm exp}(x)$, $x > x_m$. As a matching condition, we require that $\Delta_{ij}^{\rm exp}(x_m) = C_{ij} + D_{ij}x_m$ and $\frac{d}{dx}\Delta_{ij}^{\rm exp}(x_m) = D_{ij}$, i.e. we ensure that the transition between the $x \to 0$ and $M_t \gg \hat{s}, M_\Phi^2$ approximations is smooth. The matching prescription for the channels with quarks in the initial state is less intelligent due to slower convergence below threshold and the oscillating functions. Here we set $x_m = 0.9\,x_{\rm thr}$ and determine D_{ij} from the requirement $\Delta_{ij}^{\rm exp}(x_m) = C_{ij} + D_{ij}x_m$.

In Fig. 3 we show the partonic cross sections for the pseudo-scalar Higgs boson production for $M_A = 120$ GeV (left column) and $M_A = 300$ GeV (right column). The approximations obtained in the limit of large top quark mass (dashed lines) show good convergence below $x_{\rm thr}$ and diverge, as expected, for small values of x. For the gg and qg channel the matching procedure leads to good approximations to the exact results for both values of M_A. The minor differences in the gg cannel only lead to small deviations at the hadronic level. On the other hand the deviation of the matched result to the exact one in the qg channel leads to a shift of about 15% in the hadronic contributions as discussed below. At the LHC with $\sqrt{s} = 14$ TeV the contribution of the qg channel to the NNLO part of the total cross section varies between about (-8)% and (-17)% for Higgs masses between 110 GeV and 300 GeV.[6] Thus, an accuracy of 15% at NNLO induces an uncertainty of

[5] In what follows we omit the superscripts "Φ" and "(1)".

[6] These numbers are basically identical for a scalar and pseudo-scalar Higgs boson.

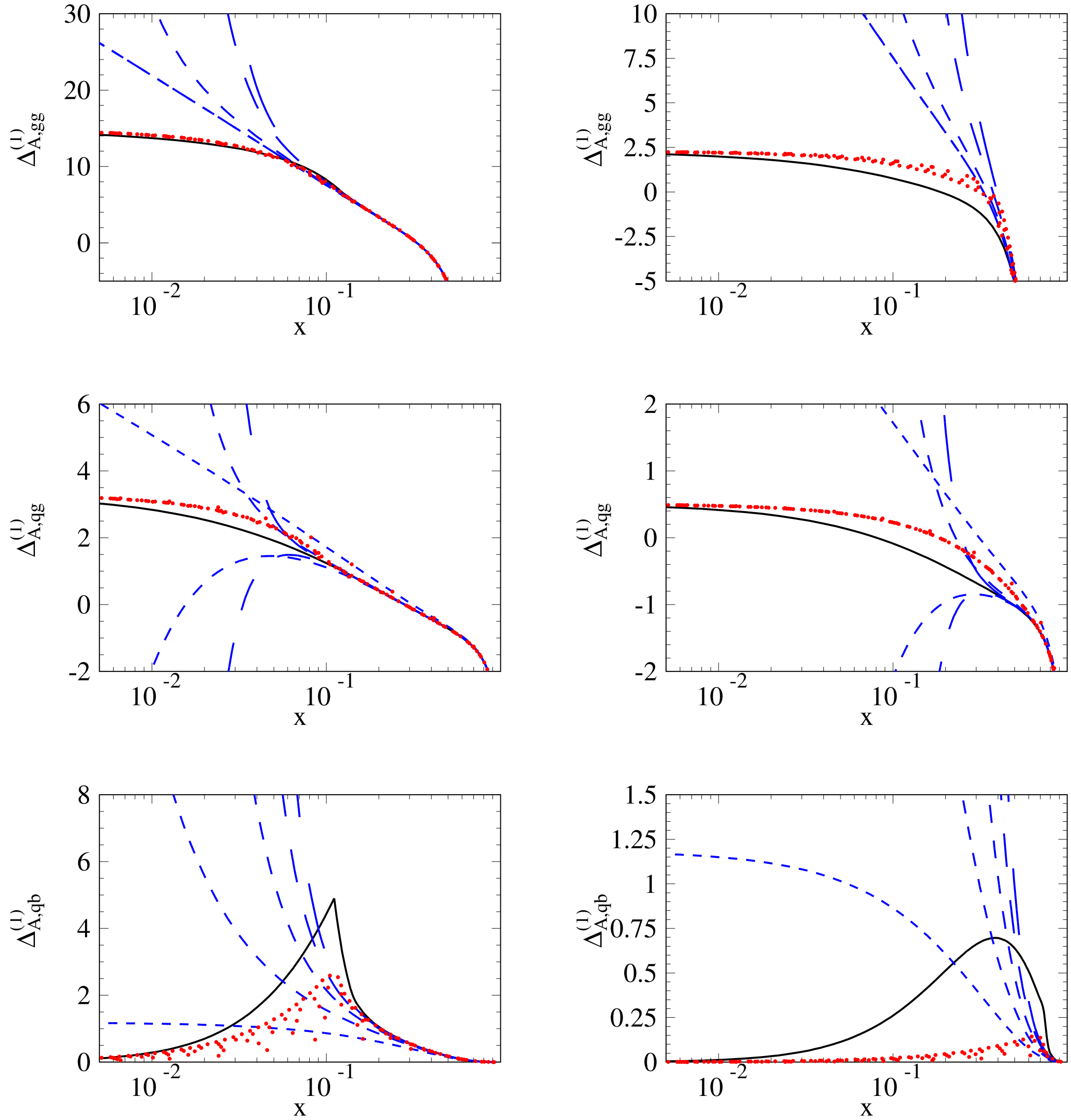

Figure 3: Partonic NLO cross sections for the gg (top), qg (middle) and $q\bar{q}$ (bottom) channel as functions of x for $M_A = 120$ GeV (left) and $M_A = 300$ GeV (right column). The expansion for $\rho \to 0$ (dashed lines) is compared with the exact result (solid lines). Lines with longer dashes include higher order terms in ρ. The interpolation results (see text) are shown as dotted lines which (for gg and qg) demonstrate an irregular structure since several lines are plotted on top of each other. The threshold values $x_{\rm thr}$ are 0.12 and 0.75, respectively. The subscript "qb" corresponds to the $q\bar{q}$ channel.

at most 3% in the NNLO piece and is hence negligible in the sum of the LO, NLO and NNLO contribution.

The situation is different for the $q\bar{q}$ channel. The partonic cross section has a charac-

ρ^n	$M_H = 120$ GeV	$M_H = 300$ GeV	$M_A = 120$ GeV	$M_A = 300$ GeV
$n = 0$	15.3696	15.3696	15.8696	15.8696
$n = 1$	+ 0.1208	+ 0.7547	+ 0.2464	+ 1.5400
$n = 2$	+ 0.0072	+ 0.2814	+ 0.0183	+ 0.7130
$n = 3$	+ 0.0005	+ 0.1296	+ 0.0016	+ 0.3896
$n = 4$	+ 0.0000	+ 0.0669	+ 0.0002	+ 0.2312
exact	15.4981	16.6956	16.1360	19.1723

Table 1: Contribution to the coefficient of $\delta(1-x)$ in the normalization of Eq. (3) from the various expansion terms $\rho^n = (M_\Phi^2/M_t^2)^n$. The renormalization scale has been set to M_Φ.

teristic peak at $x \approx x_{\rm thr}$ which is reproduced neither by the $x \to 0$ nor by the $\rho \to 0$ approximation. Due to the small contribution of this production channel (below 1% at NLO) the accuracy of the infinite-top quark mass result is sufficient.

It is worth mentioning that the quantities $\Delta_{A,ij}^{(1)}$ shown in Fig. 3 for the production of a pseudo-scalar Higgs boson are very similar to the corresponding scalar ones. This is both true for the shape and the numerical size of the corrections. For the gg channel it would not be possible to distinguish the curves for $\Delta_{gg}^{A,(1)}(x)$ and $\Delta_{gg}^{H,(1)}(x)$ for $x > 0.001$; a visible difference only occurs for $x \to 0$.

It is interesting to separately look at the δ-function contribution which is not shown in Fig. 3. In Tab. 1 we present the coefficient of $\delta(1-x)$ in the normalization of Eq. (3) both for the scalar and pseudo-scalar case. One observes that the bulk of the contribution is given by the leading term whereas the power-suppressed terms add an additional part of only 8% and 17% even for $M_\Phi = 300$ GeV in the scalar and the pseudo-scalar case, respectively. We anticipate that this behaviour is different at NNLO where the higher order terms provide more sizeable contributions as discussed in Section 4.

It is interesting to note that for $M_\Phi = 300$ GeV the sum of the first five expansion terms in Tab. 1 reproduces the exact result to better than 1% in the scalar and 2% in the pseudo-scalar case. For the latter expansion, the error can be accounted for by doubling the contribution of $n = 4$ term.

3.2 Hadronic cross section

In this subsection we compare the hadronic cross section obtained from our approximate expansions with the one obtained using the exact partonic results, implemented in `HIGLU` [45] and integrated with the same PDFs.

In Fig. 4(a) we plot the exact LO cross section as a function of M_Φ for 200 GeV $\leq M_\Phi \leq$ 400 GeV in order to demonstrate the threshold behaviour. Whereas there is a smooth transition in the scalar case, one observes a strong enhancement of the cross section for

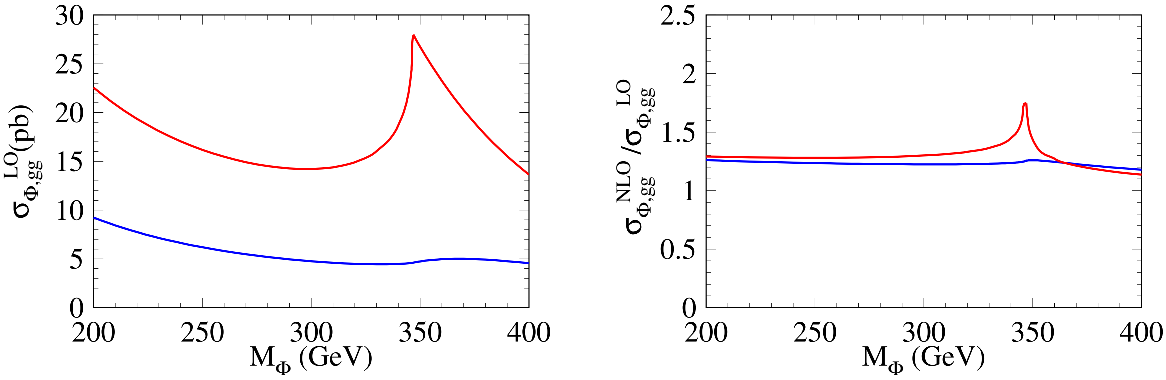

(a) (b)

Figure 4: (a) LO cross section for the production of a pseudo-scalar (top) and scalar (bottom) Higgs boson. (b) ratio of NLO and LO prediction for the total cross section. For these plots the exact results from [45] have been used.

the pseudo-scalar Higgs boson. In Fig. 4(b) the purely NLO part of the cross section is shown where the LO contribution is divided out. This is actually the quantity which is approximated by our procedure. No strong enhancement is visible for $M_A \lesssim 300$ GeV which is the upper limit considered in this paper. Thus we expect that in the pseudo-scalar case the matching procedure works as well as for the scalar one.

When discussing the quality of the matching procedure it is convenient to consider ratios of cross sections. We normalize either the exact or the matched expressions to the (unmatched) infinite-top quark mass result since these kind of ratios are also possible at NNLO. In the following plots the dashed lines represent the matched results including successively higher order in $1/M_t$ when going from short to long dahes. The solid line corresponds to the exact result.

In Fig. 5(a) the NLO gg part is shown where the factorized expressions are used in the numerator. For $M_A = 120$ GeV the deviation between the various curves is below per cent level. For $M_A = 300$ GeV, however, one observes a deviation between the exact result and the infinite-top mass approximation of about 6%. The exact result and the matched result based on the leading order deviate by about 8% whereas there is perfect agreement with the matched result including $1/M_t^8$ terms. (The corresponding dashed curve is below the solid line.)

An alternative comparison between the matched results on the one hand and the infinite-top mass and exact result on the other hand is shown in Fig. 5(b) for the gg channel where in the numerator of the considered ratio the fully expanded result is used and successively more terms in $1/M_t$ are included. A large deviation of the matched result including only the leading M_t dependence (short dashes) from the exact result is observed. However, after including higher order mass corrections in the matching procedure good agreement up to $M_A \approx 250$ GeV is observed. For Higgs boson masses close to 300 GeV a significant

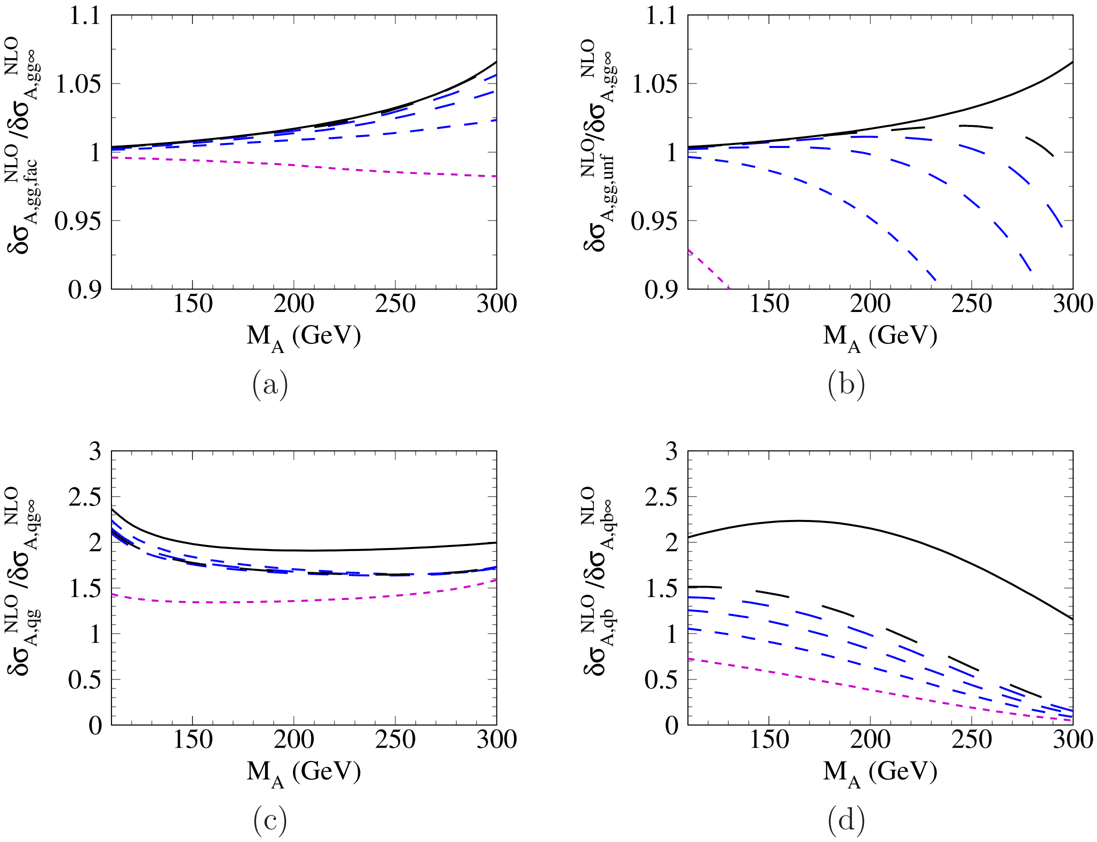

Figure 5: Ratio of the NLO parts of the hadronic cross sections for the gg (Fig. (a) and (b)), qg (Fig. (c)) and $q\bar{q}$ (Fig. (d)) channel. In (a) the exact LO result is factored out also in the matched result in the numerator whereas in (b) this option is abandoned.

deviation of the matched and exact result is visible which can be traced back to the expansion of the LO result. Thus at NNLO we adopt the approximation of Fig. 5(a) and factor the exact LO result out after including the $1/M_t$ mass corrections.

Figs. 5(c) shows the result for the qg channel. The matched result agrees with the exact one with an accuracy of about 15% whereas the infinite-top quark mass result is about a factor two smaller than the prediction based on HIGLU. For $\sqrt{s} = 14$ TeV the qg part amounts between (-2)% ($M_A = 110$ GeV) and (-7)% ($M_A = 300$ GeV) of the total NLO part. Thus, if at NNLO a similar behaviour is observed it is important to incorporate the matched qg channels in precision predictions.

As expected from the above discussion of the partonic cross section it is not possible to obtain a good approximation to the exact result for the $q\bar{q}$ channel which is shown in Fig. 5(d). For lower pseudo-scalar Higgs boson masses there is also a significant deviation between the exact and the infinite-top mass result, for $M_A = 300$ GeV, however, they (accidentally, as can be seen in the lower right panel of Fig. 3) agree perfectly well.

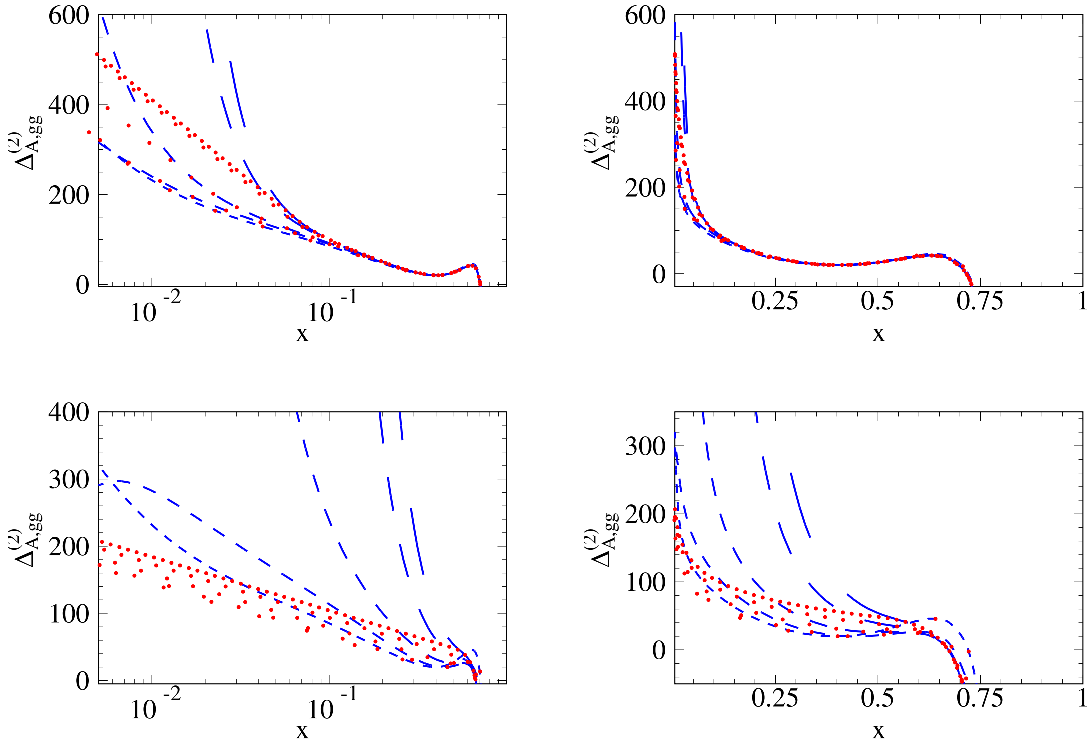

Figure 6: Partonic cross section for the gg channel for $M_A = 120$ GeV (top) and $M_A = 300$ GeV (bottom). The plots on the left employ a logarithmic and on the right a linear x-scale. The notation is adopted from Fig. 3.

4 Partonic NNLO cross section

In this Section we discuss the partonic cross sections for the various channels at NNLO. We follow the matching procedure outlined in Section 3.1 for the NLO calculation, with minor modifications due to the different $x \to 0$ limit. At the NNLO[7]

$$\Delta_{ij}(x) \stackrel{x \to 0}{=} E_{ij} \ln x + \mathcal{O}(1)\,, \tag{24}$$

and Ref. [22] provides coefficients E_{ij}. We again choose the matching value $x_m \sim x_{\rm thr}$ such that the transition between the $x \to 0$ and $M_t^2 \gg \hat{s}, M_\Phi^2$ approximations is smooth: $\Delta_{ij}^{\rm exp}(x_m) = E_{ij} \ln x_m + F_{ij}$, $\frac{d}{dx}\Delta_{ij}^{\rm exp}(x_m) = E_{ij}/x_m$, and $\Delta_{ij}^{\rm exp}(x_m)$ is given in Eq. (22).

This prescription applies to the gg channel. For the other initial states we again use $x_m = 0.9\, x_{\rm thr}$ and require that $\Delta_{ij}^{\rm exp}(x_m)$ agree with the corresponding infinite-energy result.

In Fig. 6 we show the partonic cross section for the numerically most important gg channel at $M_A = 120$ GeV and $M_A = 300$ GeV, with linear and logarithmic scales of the x axis.

[7] We again omit the superscripts "Φ" and "(2)".

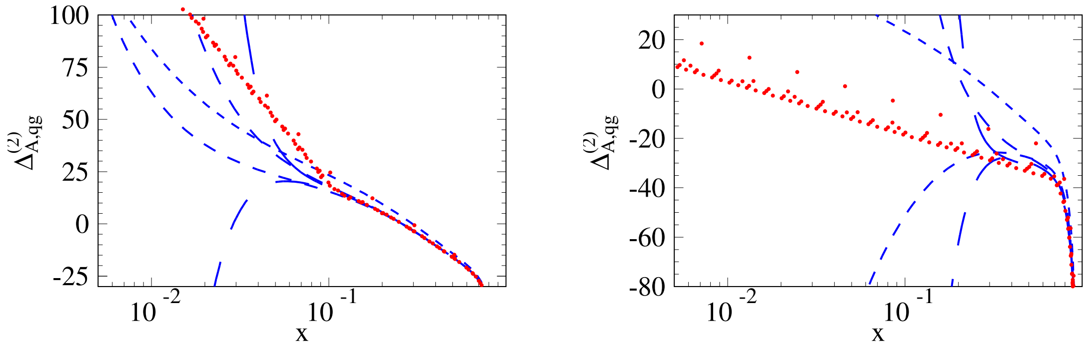

Figure 7: Partonic cross section for the qg channel for $M_A = 120$ GeV (left) and $M_A = 300$ GeV (right panel). The notation is adopted from Fig. 3.

The dashed lines represent the results for $\sigma_{ij}^{\rm exp}$ (cf. Eq. (22)); longer dashes indicate higher order ρ-expansion. As expected, these results diverge for $x < x_{\rm thr}$. The results interpolated as described above are shown with dotted lines, shorter distances between the dots correspond to higher-order ρ-expansion in the matching procedure.

For $M_A = 120$ GeV the partonic cross section has a maximum at $x \approx 0.6$ which is significantly higher than $x_{\rm thr} \approx 0.12$ and thus it is nicely reproduced from $\sigma_{ij}^{\rm exp}$. The approximations start diverging at $x \approx x_{\rm thr}$. As far as the matched results are concerned one observes stabilization starting from the one including the ρ^2 terms.

For $M_A = 300$ GeV we have $x_{\rm thr} \approx 0.75$ which is close to the steep rise of the partonic cross section. The expansion results show good convergence properties down to $x \approx 0.6$ and start to diverge around $x = 0.45$, significantly below $x_{\rm thr}$. As far as the matched results are concerned a similar behaviour as for $M_A = 120$ GeV is observed: The inclusion of higher order terms in ρ stabilizes the matching procedure, leading to firm NNLO results for the partonic cross section.

Let us next discuss the qg-initiated partonic cross section shown in Fig. 7 for $M_A = 120$ GeV and $M_A = 300$ GeV. Again, very nice convergence happens at $x > x_{\rm thr}$ and the matching to $\hat{s} \to \infty$ results is rather stable. The approximation is shown with dotted lines, the shorter distances between the dots denote higher-order terms in ρ. One observes that the latter are important for reliable results. Both for $M_A = 120$ GeV and $M_A = 300$ GeV there is a visible difference between the curves including only ρ^0 terms and the $\mathcal{O}(\rho)$ result. Further corrections are relatively small. Judging from the behaviour at NLO it can be expected that the results for the partonic qg channel approximate the (unknown) exact result quite well with an uncertainty below 15%.

The matching procedure was also applied to the quark-initiated processes $q\bar{q}$, qq and qq'. We show the results in Fig. 8 using the same notation as in Fig. 6. For the $q\bar{q}$ we expect a peculiar structure similar to the one at NLO (cf. Fig. 3) which is not reproduced by our procedure. However, since the overall contribution from this channel is small, we may

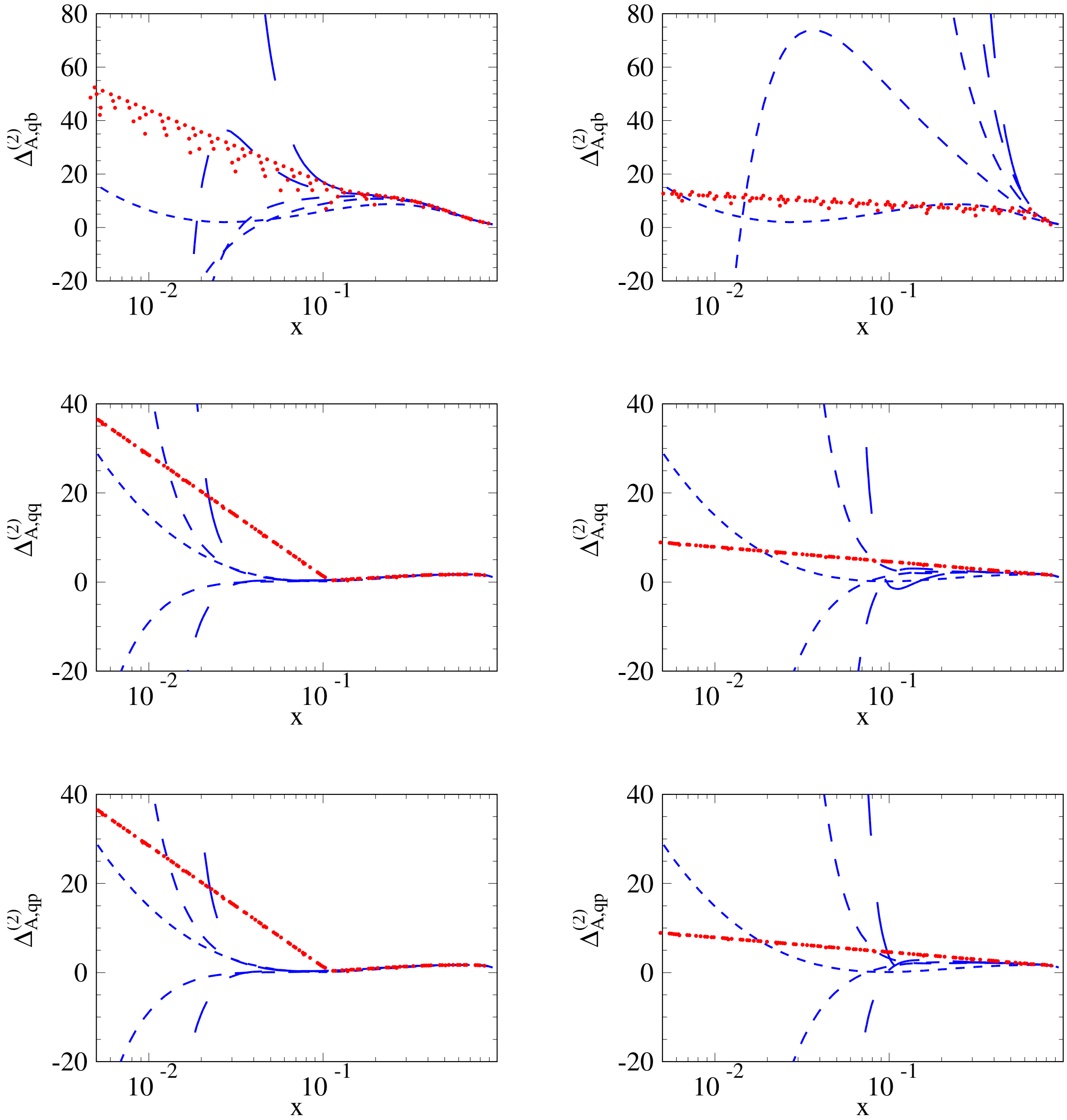

Figure 8: Partonic cross section for the $q\bar{q}$ ("qb"), qq and qq' ("qp") channels for $M_A = 120$ GeV (left) and $M_A = 300$ GeV (right). The notation is adopted from Fig. 3.

neglect the uncertainty of the matching procedure.

The numerical contribution from the qq and qq' channels to the total hadronic cross section is similar to the $q\bar{q}$ one. For these initial states, however, we do not expect a complicated shape of the curves and thus the matched result through ρ^4 terms can be trusted both for $M_A = 120$ GeV and $M_A = 300$ GeV. (The differences between the various matched results are again small at the hadronic level.)

By analogy to Tab. 1, in Tab. 2 we present the NNLO contribution to the δ-function part

ρ^n	$M_H = 120$ GeV	$M_H = 300$ GeV	$M_A = 120$ GeV	$M_A = 300$ GeV
$n = 0$	83.5654	94.0264	95.9237	105.0866
$n = 1$	+ 3.5586	+ 24.0520	+ 6.5340	+ 44.7899
$n = 2$	+ 0.2190	+ 9.1031	+ 0.5330	+ 22.5153
$n = 3$	+ 0.0164	+ 4.2818	+ 0.0495	+ 13.0672
$n = 4$	—	—	+ 0.0050	+ 8.1572

Table 2: NNLO contribution to the coefficient of $\delta(1-x)$ in the normalization of Eq. (3) from the various expansion terms $\rho^n = (M_\Phi^2/M_t^2)^n$. The renormalization scale has been set to M_Φ.

which is not contained in the plots discussed before. For $M_A = 120$ GeV the convergence is fast. The ρ terms still provide about 7%, however, already the ρ^2 terms are below 1%. At $M_A = 300$ GeV a good approximation to the exact result requires terms through ρ^4. Estimating the contribution of the ρ^n terms for $n \geq 5$ as twice the ρ^4 contribution, we expect the accuracy of about 8%. For $M_A = 280$ GeV this number goes down to 5%.

Since the analytic results are quite lengthy we refrain from listing them here explicitly. They are available on request from the authors.

5 Hadronic cross sections

In this Section we present the hadronic cross section for the individual channels and compare in each case with the infinite-top quark mass approximation in order to quantify the accuracy of the latter. Although the results for the scalar Higgs boson have already been discussed in the literature [18–20] we present results both for the scalar and pseudo-scalar case for comparisons. For the numerical results we use the nominal LHC center-of-mass energy $\sqrt{s} = 14$ TeV; for $\sqrt{s} = 7$ TeV the results look qualitatively very similar.

Let us again start with the gg-induced channel. In Fig. 9 the ratio

$$\frac{\delta\sigma_{gg}^{\mathrm{NNLO}}}{\delta\sigma_{gg,\infty}^{\mathrm{NNLO}}} \tag{25}$$

of the NNLO contribution to the total cross section is shown. In the numerator the matched partonic results are used and in the denominator is the bare infinite-top quark mass result. As before, the lines with longer dashes include higher expansion terms in ρ. Note that for the scalar Higgs boson terms through ρ^3 are available whereas for the pseudo-scalar case we could compute even the ρ^4 terms. Actually, in the practical calculation it turns out that the diagrams with pseudo-scalar couplings lead to significantly fewer terms at the intermediate steps. We believe that this is due to elimination of many terms with anti-symmetric properties of the ϵ-tensors remaining after the γ_5-matrices.

In the left column the exact LO result is factored out both in the numerator and the denominator[8]. One observes that the correction for the pseudo-scalar Higgs boson is between 2.5% for $M_A = 120$ GeV and about 20% for $M_A = 300$ GeV which is significantly larger than for the scalar Higgs boson, reaching at most 9% [18–20]. Judging from the difference of the two consecutive curves, we observe in both cases good convergence of the ρ-expansion even for $M_A = 300$ GeV. This gives us some confidence that the corrections including the highest powers in ρ are approaching the unknown exact result.

The right panels in Fig. 9 show the ratio (25) with the numerator expanded in ρ without factoring out the LO mass dependence. The plot for the scalar Higgs boson reproduces the results in the literature [18–20], demonstrating that after including higher orders in ρ the ratio becomes less dependent of M_Φ. The curve including ρ^3 terms deviates from unity at most by about 5%. The situation is different for the pseudo-scalar case. For low Higgs boson masses the corrections also converge against a few per cent, for higher mass values, however, they amount up to about 10% demonstrating that the infinite-top mass result accompanied by the matching procedure is not sufficient to approximate the exact result with 1% accuracy or better.

Similarly to the NLO case shown in Fig. 5 we observe also in Fig. 9 that the convergence becomes poor for Higgs boson masses above 250 GeV if the exact LO mass dependence is not factored out. Thus, for our final prediction we use the approach of the upper left plot in Fig. 5 where the effect of higher order terms in ρ (beyond ρ^4) can be safely neglected.

The hadronic cross section for the quark-induced channels, qg, $q\bar{q}$, qq and qq' are shown in Fig. 10 with the notation similar to Fig. 9. In all cases we observe decent convergence with higher ρ powers. From the NLO analyses of Section 3 we expect that the prediction for the qg channel agrees with the exact result to within about 15%. Note that there is a noteable correction from including the first ρ-suppressed term. This behaviour can be explained by the pattern in corresponding partonic cross section discussed in the previous Section (see Fig. 7).

As far as the $q\bar{q}$ channel is concerned, the matched results coincide with the effective-theory prediction within roughly a factor of two to three for 120 GeV $< M_A <$ 250 GeV which decreases to about 1.2 for $M_A = 300$ GeV. The results for the qq and qq' channels are shown for completeness in the bottom row of Fig. 10. The deviation between the matched and the effective-theory result in the considered Higgs boson mass range is about 1.5 to 2. For $\sqrt{s} = 14$ TeV the overall contribution from the qg, $q\bar{q}$, qq and qq' channels to the NNLO corrections amounts to (-8)% to (-17)%, 0.1% to 0.2%, 0.08% and 0.3%, respectively. Thus, at the current level of accuracy it is certainly possible to use the infinite-top quark mass result for the predictions originating from the $q\bar{q}$, qq and qq' channels. For $M_A = 300$ GeV the infinite-top quark mass approximation for the qg channel may lead to an uncertainty of about 2% in the NNLO prediction of the hadronic cross section.

[8]The slight deviation from unity of the curve including only the ρ^0 term is due to matching effects.

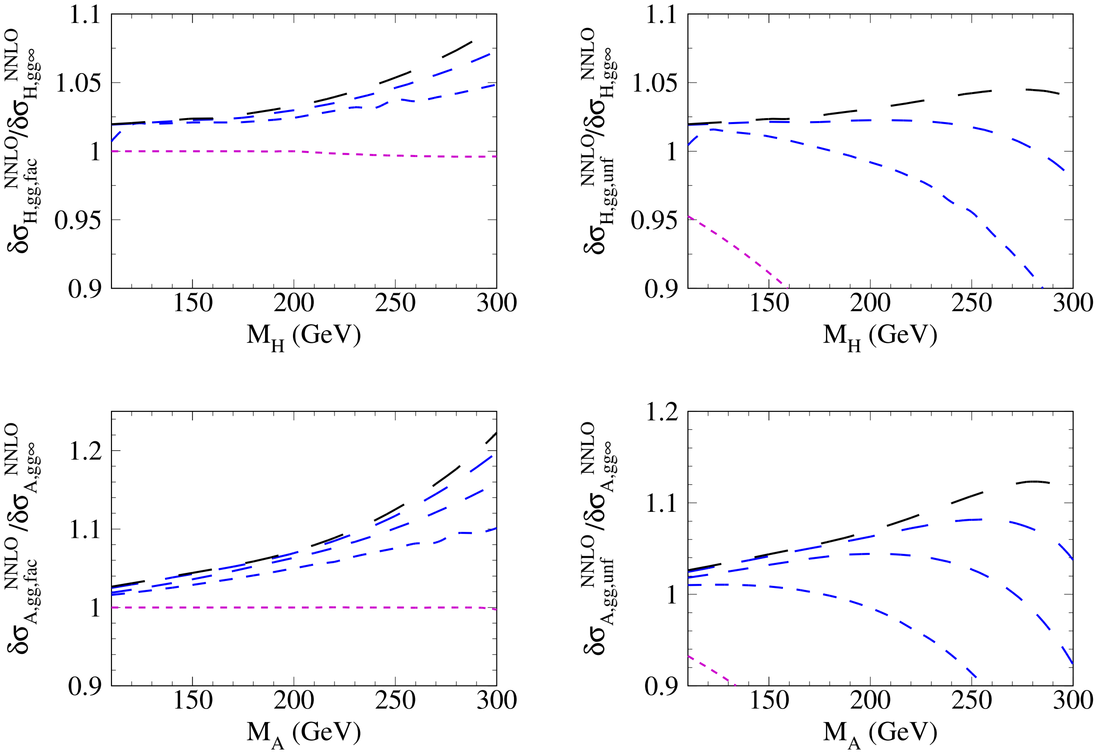

Figure 9: NNLO contribution to the hadronic cross section of the gg-channel normalized to the infinite-top quark mass result. Top: scalar Higgs boson; bottom: pseudo-scalar Higgs boson. The left plots the exact LO result is factorized whereas in the right plots no factorization is used.

It is instructive to look at the individual contributions of the NNLO pieces to the hadronic cross section. In Tab. 3 we show for $M_\Phi = 300$ GeV the contributions from the δ function, the plus distributions and the remainder. The infinite-top mass result is confronted with the approximations based on the matching that incorporates corrections of order ρ^n $(n = 0, 1, \ldots)$. One observes that both for the scalar and the pseudo-scalar Higgs boson the virtual corrections grow by almost a factor of two compared to the infinite-top mass values. In both cases the contribution from the plus distributions are quite small and the contribution from the δ function amounts to about a quarter of the remainder. The latter dominate the corrections and amount to about 85% in the scalar and about 80% in the pseudo-scalar case. The difference between the best prediction and the infinite-top corrections amounts to 9% and 22%, respectively.

For the M_Φ values below 300 GeV the convergence of all individual contributions significantly improves and our error estimate (given by the size of the last known term) is below 2% and thus is negligible.

Let us finally show results for the cross section of the numerically dominant gg-induced contribution. In Fig. 11 the LO, NLO and NNLO predictions for the total production

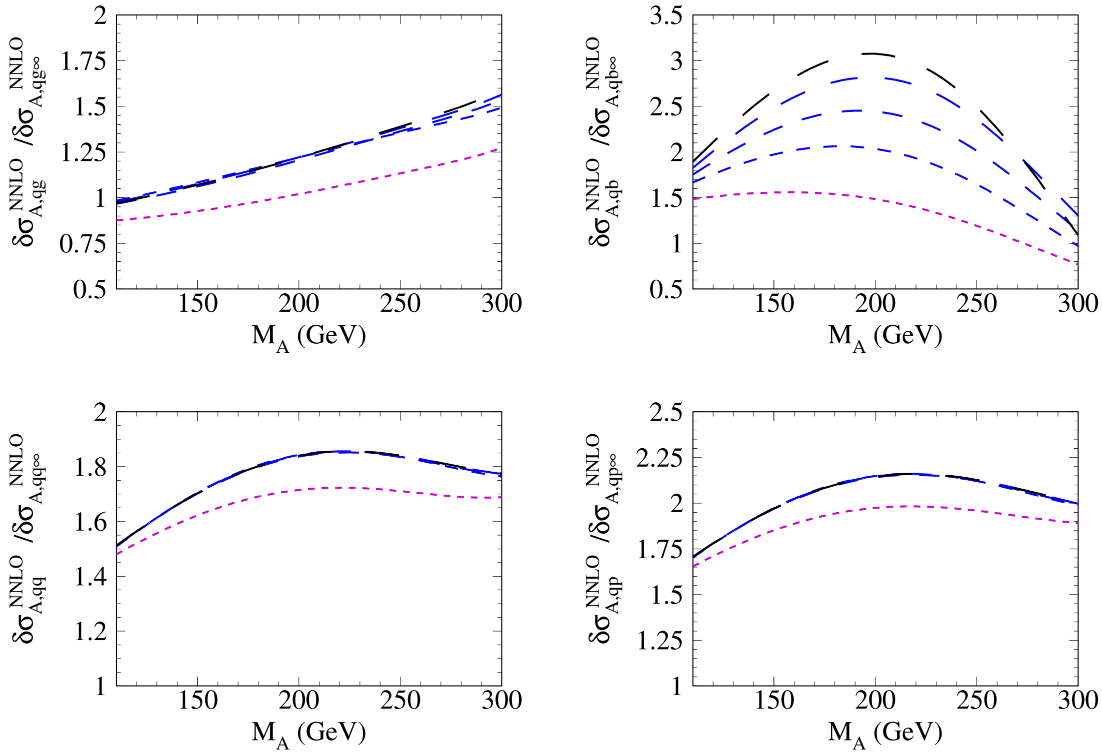

Figure 10: NNLO contribution to the hadronic cross section for the inclusive production of a pseudo-scalar Higgs boson induced by the "qg", "$q\bar{q}$", "qq" and "qq'" channels.

H	$\delta(1-x)$	$[\ldots]_+$	rest
$M_t \to \infty$	0.363	−0.066	2.555
"0"	0.363	−0.066	2.544
"1-0"	0.093	0.002	0.054
"2-1"	0.035	0.001	0.034
"3-2"	0.017	0.000	0.034
"3"	0.508	−0.063	2.666

A	$\delta(1-x)$	$[\ldots]_+$	rest
$M_t \to \infty$	1.213	−0.194	7.728
"0"	1.213	−0.194	7.703
"1-0"	0.517	0.013	0.380
"2-1"	0.260	0.006	0.236
"3-2"	0.151	0.003	0.185
"4-3"	0.094	0.002	0.128
"4"	2.235	−0.170	8.633

Table 3: Individual contributions to the quantity $\delta\sigma^{\rm NNLO}_{\Phi,gg}$ (i.e. the gg induced part) in Eq. (20) for $M_\Phi = 300$ GeV for a scalar (left) and pseudo-scalar Higgs boson (right). The first line corresponds to the infinite-top quark mass result and "i" represents the matched result including terms of order ρ^i. The bottom line contains the best available prediction.

cross section both for a scalar (left) and a pseudo-scalar Higgs boson (right) is plotted. The dotted and the dash-dotted lines belong to the exact LO and NLO prediction and the solid lines represent our best NNLO expression, i.e. the matched cross section containing the ρ^3 and ρ^4 corrections for the scalar and pseudo-scalar Higgs boson, respectively. For comparison we also show as the dashed line the result which is obtained if the infinite-top

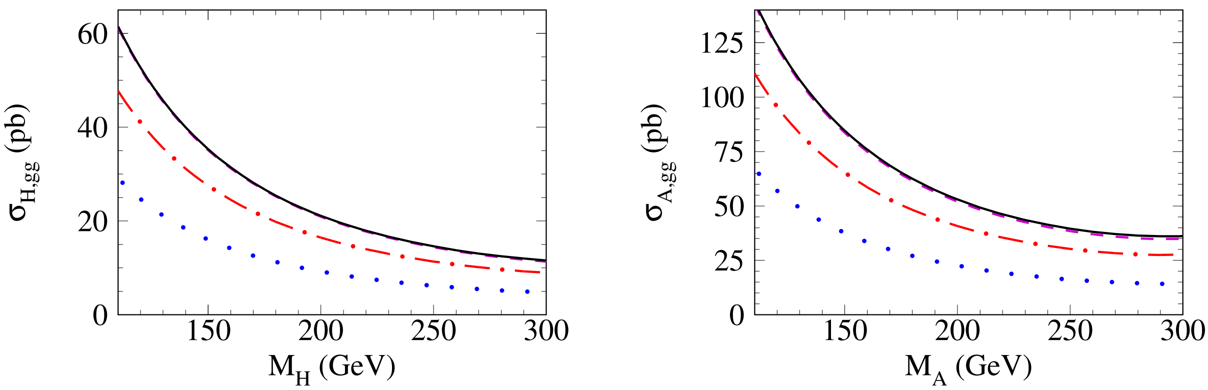

Figure 11: Total cross section for the production of a scalar (left) and pseudo-scalar (right) Higgs boson to LO (dotted), NLO (dash-dotted) and NNLO (solid) precision. The dashed line corresponds to the prediction where for the NNLO corrections the heavy-top approximation has been used.

quark mass approximation is used for the NNLO term. In the scalar case one barely sees a difference with the solid line whereas for the pseudo-scalar Higgs boson there is a deviation of about 6% for masses around 300 GeV. Thus it is important to replace the infinite-top mass results in this Higgs boson mass region by the matched results presented in this paper in future precision studies.

6 Conclusions

In this paper we consider the inclusive production of the scalar and the pseudo-scalar Higgs boson at hadron colliders. We compute the NNLO production cross section for Higgs bosons with masses below approximately 300 GeV, including top quark mass effects. The technique that we use extends the method that was recently applied to scalar Higgs boson production to the pseudo-scalar case. It relies on an asymptotic expansion in the limit of a large top quark mass and a subsequent matching to the zero-mass limit. This paper contains a detailed description of the method and several intermediate results which could be useful in the context of other calculations. In particular we provide all one- and two-loop four-point master integrals with an ϵ expansion sufficient for a N^{3}LO calculation.

The main conclusions of our NNLO analysis are as follows.

- At NLO our approach reproduces the exact result with high precision (see discussion in Section 3).
- Since at NLO the agreement between our approximation and the exact result is below 1% for the gg channel once expansion terms up to order $1/M_t^8$ are included

we are quite confident that the same is true at NNLO. Thus, from the practical point of view our calculation is equivalent to the exact one (at least for Higgs boson masses below threshold).

- Our NNLO corrections deviate from the infinite-top quark mass approximation (with exact LO mass dependence factored out) by about 2% for low Higgs boson masses. For higher masses the deviation is larger. For $M_\Phi = 300$ GeV it amounts to about 9% for the scalar Higgs boson and about 22% for the pseudo-scalar case.

- This leads to the conclusion that up to an uncertainty of about 2% for the scalar case and about 6% for the pseudo-scalar case it is save to use the infinite-top quark mass approximation [13–17] for the prediction of the total cross section. This is a non-trivial result which so far has no fundamental explanation.

  In case one aims for a better precision the infinite-top quark mass results have to be replaced by the results presented in this paper.

- The accuracy of the NNLO part of the infinite-top quark mass result for $M_\Phi = 300$ GeV amounts to 6% (15%) for the scalar (pseudo-scalar) case at Tevatron. For the LHC with $\sqrt{s} = 7$ TeV the numbers are 8% and 20%.

For Higgs boson masses above approximately two times the top quark mass the approximation used for the asymptotic expansion is not justified. In this limit one has to rely on the good agreement between the exact and the infinite-top mass result at NLO and assume that it extends to NNLO.

Acknowledgements

This work was supported by the DFG through the SFB/TR 9 "Computational Particle Physics". We would like to thank Fabrizio Caola and Simone Marzani for providing us with detailed numerical results for the NNLO production cross section in the infinite-energy limit.

A Two-loop four-point master integrals

The one- and two-loop four-point integrals have been studied for the first time in Ref. [14] (see Appendix B). Unfortunately, that reference contains a number of misprints. We independently evaluated these integrals by a combination of soft expansion[9] and differential equation methods. We furthermore extend the results of Ref. [14] by adding more terms in ϵ which are required for a third-order calculation of the Higgs boson production cross section. The results can be downloaded in `Mathematica` format from the webpage [46].

[9]We acknowledge help with cross checks of the soft expansion by Robert Harlander and Kemal Ozeren.

The integrals published in Ref. [14] suffer from multiple typographical errors. We have also found a number of less trivial inaccuracies. In particular, the integral of Eq. (B.3) is off by a factor of 2, the right-hand side of Eq. (B.27) must read

$$= \mathcal{P}^2 z^{-2\epsilon} \left[\frac{\log(z)^2}{2\epsilon} - 4\zeta_3 - 4\zeta_2 \log(z) + 4\mathrm{Li}_3(z) + \frac{\log^3(z)}{2} - 2\log^2(z) + \mathcal{O}(\epsilon) \right], \tag{26}$$

the right-hand side of Eq. (B.22) should begin with

$$= \mathcal{P}^2 z^{-\epsilon}(1-z)^{-2\epsilon} \left\{ \mathrm{Li}_2(1-z) + \frac{\log^2(z)}{2} + ... \right\}, \tag{27}$$

the two terms $-4\log(1-z)^2 - 8$ of the $\mathcal{O}(\epsilon^0)$ contribution in Eq. (B.21) must be replaced with $+4\log(1-z)^2 + 8$, etc.

B Convolution of partonic cross section and splitting functions

The singularities associated with the collinear radiation of quarks and gluons from the incoming partons are described by convolutions of the partonic cross sections $\sigma_{ij}(x)$ with the splitting functions $P_{jk}(x)$ where a convolution of the two functions $f(x)$ and $g(x)$ is defined as

$$[f \otimes g](x) = \int_0^1 \mathrm{d}x_1 \mathrm{d}x_2 \delta(x - x_1 x_2) f(x_1) g(x_2). \tag{28}$$

The functions that appear in the LO, NLO, and NNLO cross sections and LO and NLO splitting functions include combinations of HPLs of weight one, two, and three with the factors x, $1-x$, and $1+x$, and the generalized functions $\delta(1-x)$ and $\left[\frac{\ln^k(1-x)}{1-x}\right]_+$. It is convenient to transform those functions to the Mellin space, where the convolutions turn into products of Mellin images:

$$M_n[f(x)] = \int_0^1 x^{n-1} f(x) dx, \tag{29}$$

$$M_n[[f \otimes g](x)] = M_n[f(x)]\, M_n[g(x)]. \tag{30}$$

The Mellin transforms of various functions present in the NNLO Higgs boson production were studied in the literature [47]. We, however, decided to relate all required results to a limited set of Mellin transforms of HPLs with a certain maximum weight.

Let us consider the Mellin transforms of HPLs of weight zero and one:

$$\begin{aligned}
M_n[1] &= \frac{1}{n}\,, \\
M_n[\mathrm{H}_0(x)] &= -\frac{1}{n^2}\,, \\
M_n[\mathrm{H}_1(x)] &= \frac{\mathrm{S}_1(n)}{n}\,, \\
M_n[\mathrm{H}_{-1}(x)] &= -\frac{(-1)^n}{n}\left(\mathrm{S}_{-1}(n)+\ln 2\right)+\frac{\ln 2}{n}\,,
\end{aligned} \tag{31}$$

where H_i are the HPLs of weight 1 [48]. The harmonic sums $\mathrm{S}_{...}(n)$ are defined as follows:

$$\mathrm{S}(n)=1,\quad \mathrm{S}_{a,\vec{b}}(n)=\sum_{i=1}^{n} f_a(i)\ \mathrm{S}_{\vec{b}}(i),\quad f_a(i)=\begin{cases} i^{-a}, & a\geq 0\,, \\ (-1)^i\ i^a, & a<0\,. \end{cases} \tag{32}$$

One may define the weight of those sums as the sum of the absolute values of their indices.

Similarly to Eqs. (31), Mellin images of HPLs of higher weights contain harmonic sums of higher weights and various transcendental numbers originating from various HPLs evaluated at $x=1$. We choose the representations where each Mellin image contains only n as the argument of sums and integer powers of n in the denominators, and no products of sums (the corresponding algebra is discussed later).

Some related Mellin transforms can be found by index shifting and integration by parts:

$$M_n\left[x^k f(x)\right] = M_{n+k}\left[f(x)\right], \tag{33}$$

$$M_n\left[\frac{d}{dx}f(x)\right] = x^n f(x)|_0^1-(n-1)M_{n-1}\left[f(x)\right]. \tag{34}$$

In the latter relation, the boundary term has to be properly defined. In the limit $x\to 0$ it vanishes since we always consider n higher than the order of the highest pole that $f(x)$ may have at $x=0$. If $f(x)$ is some HPL, then its limit at $x\to 1$ may be either zero, a non-zero constant, or singular as $\ln^k(1-x)$. Such a singularity is present e.g. in $\mathrm{H}_1(x)=-\ln(1-x)$, so that Mellin transform of $\frac{d}{dx}\mathrm{H}_1(x)=\frac{1}{1-x}$ does not exist. On the other hand, such functions can be regularized by turning them into a plus-distribution, and $\left[\frac{1}{1-x}\right]_+$ has a well-defined Mellin transform, $-\mathrm{S}_1(n-1)$. We notice that this result can be obtained if we artificially drop the logarithmically divergent contributions from the boundary term in Eq. (34). In general, we may define the regularized derivative $\hat{\partial}_x$ acting as follows:

$$M_n\left[\hat{\partial}_x f(x)\right]=R\left[f(x)\right]-(n-1)M_{n-1}\left[f(x)\right] \tag{35}$$

where

$$\begin{aligned}
&R[g_a(x)\ln^a(1-x)+g_b(x)\ln^b(1-x)+...+g_0(x)]=g_0(1)\,, \\
&a,b,...>0,\quad g_k(1)\neq 0\ \ \forall k>0\,.
\end{aligned} \tag{36}$$

The extraction of divergent logarithms from HPLs is implemented e.g. in the function `HPLLogExtract` of the HPL.m package [48].

Using this definition and the inverse Mellin transform, we may establish relations between the derivatives of HPLs and the common generalized functions:

$$\begin{aligned}
\hat{\partial}_x\, 1 &= \delta(1-x), \\
\hat{\partial}_x \mathrm{H}_1(x) &= \left[\frac{1}{1-x}\right]_+, \\
\hat{\partial}_x \mathrm{H}_{11}(x) &= -\left[\frac{\ln(1-x)}{1-x}\right]_+, \\
\hat{\partial}_x \mathrm{H}_{111}(x) &= \frac{1}{2}\left[\frac{\ln^2(1-x)}{1-x}\right]_+, \\
\hat{\partial}_x \mathrm{H}_{101}(x) &= \frac{\pi^2}{6}\left[\frac{1}{1-x}\right]_+ + \frac{\mathrm{H}_{01}(x)-\zeta_2}{1-x}, \quad \text{etc.}
\end{aligned} \tag{37}$$

Thus, it is not necessary to separately consider Mellin images of functions related to the derivatives of HPLs, such as $\frac{\mathrm{H}_{\dots}(x)}{1+x}$, $\left[\frac{\mathrm{H}_{\dots}(x)}{1-x}\right]_+$, etc.

At a given weight of sums, one may interpret the relations obtained by extending Eq. (31) as a system of equations, and complete it with the generalized derivatives of every line (excluding trivial relations). It is possible to solve this system for the monomials $1/n^k$, $\mathrm{S}_{\dots}(n)/n^k$, and $(-1)^n\mathrm{S}_{\dots}(n)/n^k$ in order to determine their inverse Mellin transforms. While writing this paper, we have learned about the work [49] that in particular mentions some very general algorithms to compute Mellin images of HPLs of arbitrary weights. Unfortunately, at this moment the program implementing those algorithms is not yet available to the public.

If a Mellin image that we deal with is a linear combination of such known terms (with possibly shifted indices), its inverse transform is trivial to find with the help of the linearity of $M_n[f(x)]$ and Eq. (33). However, to find the convolution of two functions we need to multiply the two Mellin images and the resulting terms may have a more complicated structure. Nevertheless, it is possible to transform the expressions to the required shape.

First, the factorized denominators $(n+a)^{-i}(n+b)^{-j}\dots$ must be decomposed by partial fractioning. Second, the arguments of harmonic sums must be brought to agreement with the denominators using the definition Eq. (32): $\mathrm{S}_{a,\vec{b}}(n+1) = \mathrm{S}_{a,\vec{b}}(n) + f_a(n+1)\mathrm{S}_{\vec{b}}(n+1)$. Finally, the products of sums must be transformed into linear combinations of sums of higher orders. The corresponding algebra originates from the obvious identity

$$\left(\sum_{i=1}^{n} a_i\right)\left(\sum_{j=1}^{n} b_j\right) = \sum_{i=1}^{n}\left(a_i \sum_{j=1}^{i} b_j\right) + \sum_{i=1}^{n}\left(b_i \sum_{j=1}^{i} a_j\right) - \sum_{i=1}^{n}(a_i b_i)\,, \tag{38}$$

which is applied recursively. For every product, it is then possible to arrive at the decomposition such as $\mathrm{S}_{-1,2}(n)\mathrm{S}_{-1}(n) = 2\mathrm{S}_{-1,-1,2}(n) + \mathrm{S}_{-1,2,-1}(n) - \mathrm{S}_{-1,-3}(n) - \mathrm{S}_{2,2}(n)$.

The above algorithm has been implemented as a Mathematica program. Since the HPL package [48] is not capable of computing integrals Eq. (29) with arbitrary n, the table of Mellin transforms (similar to Eq. (31)) has to be pre-computed. The regular form of the relations Eq. (31) and the further results greatly simplifies the solution. We have been able to compile the table for the transforms of HPLs up to weight five, which should be sufficient to evaluate convolutions relevant to the NNNLO correction to the Higgs boson production. For that purpose one has to consider among other contributions the convolution of the NNLO partonic gg-induced cross section with the LO splitting function. The former contains contributions like $H_{010}(x)/(1-x)$ which can be written in terms of generalized derivatives of HPLs of weight 4. The LO splitting function has contributions from HPLs of weight 1 thus resulting in quantities of weight 5. Similary, the convolution of the NLO partonic cross section with the NLO splitting function involves HPLs of weight 2 and 3, respectively, again leading to HPLs of weight 5.

References

[1] R. Barate *et al.* [LEP Working Group for Higgs boson searches and ALEPH Collaboration and and], Phys. Lett. B **565** (2003) 61 [arXiv:hep-ex/0306033].

[2] T. Aaltonen *et al.* [CDF and D0 Collaboration], arXiv:1103.3233 [hep-ex].

[3] J. Baglio, A. Djouadi, S. Ferrag and R. M. Godbole, Phys. Lett. B **699** (2011) 368 [arXiv:1101.1832 [hep-ph]].

[4] F. Wilczek, Phys. Rev. Lett. **39** (1977) 1304.

[5] J. R. Ellis, M. K. Gaillard, D. V. Nanopoulos and C. T. Sachrajda, Phys. Lett. B **83** (1979) 339.

[6] H. M. Georgi, S. L. Glashow, M. E. Machacek and D. V. Nanopoulos, Phys. Rev. Lett. **40** (1978) 692.

[7] T. G. Rizzo, Phys. Rev. D **22** (1980) 178 [Addendum-ibid. D **22** (1980) 1824].

[8] S. Dawson, Nucl. Phys. B **359** (1991) 283.

[9] A. Djouadi, M. Spira and P. M. Zerwas, Phys. Lett. B **264** (1991) 440.

[10] M. Spira, A. Djouadi, D. Graudenz and P. M. Zerwas, Nucl. Phys. B **453** (1995) 17, arXiv:hep-ph/9504378.

[11] R. Harlander and P. Kant, JHEP **0512** (2005) 015 [arXiv:hep-ph/0509189].

[12] R. V. Harlander, Phys. Lett. B **492** (2000) 74, arXiv:hep-ph/0007289.

[13] R. V. Harlander and W. B. Kilgore, Phys. Rev. Lett. **88** (2002) 201801, arXiv:hep-ph/0201206.

[14] C. Anastasiou and K. Melnikov, Nucl. Phys. B **646** (2002) 220, arXiv:hep-ph/0207004.

[15] V. Ravindran, J. Smith and W. L. van Neerven, Nucl. Phys. B **665** (2003) 325, arXiv:hep-ph/0302135.

[16] R. V. Harlander and W. B. Kilgore, JHEP **0210** (2002) 017 [arXiv:hep-ph/0208096].

[17] C. Anastasiou and K. Melnikov, Phys. Rev. D **67** (2003) 037501 [arXiv:hep-ph/0208115].

[18] R. V. Harlander and K. J. Ozeren, JHEP **11** (2009) 088, arXiv:0909.3420 [hep-ph].

[19] A. Pak, M. Rogal and M. Steinhauser, JHEP **1002** (2010) 025 [arXiv:0911.4662 [hep-ph]].

[20] R. V. Harlander, H. Mantler, S. Marzani and K. J. Ozeren, Eur. Phys. J. C **66** (2010) 359 [arXiv:0912.2104 [hep-ph]].

[21] S. Marzani, R. D. Ball, V. Del Duca, S. Forte and A. Vicini, Nucl. Phys. B **800** (2008) 127 [arXiv:0801.2544 [hep-ph]].

[22] F. Caola and S. Marzani, Phys. Lett. B **698** (2011) 275 [arXiv:1101.3975 [hep-ph]].

[23] S. Catani, D. de Florian, M. Grazzini and P. Nason, JHEP **0307** (2003) 028, arXiv:hep-ph/0306211.

[24] S. Moch and A. Vogt, Phys. Lett. B **631** (2005) 48 [arXiv:hep-ph/0508265].

[25] V. Ravindran, Nucl. Phys. B **746** (2006) 58 [arXiv:hep-ph/0512249].

[26] V. Ravindran, Nucl. Phys. B **752** (2006) 173 [arXiv:hep-ph/0603041].

[27] V. Ahrens, T. Becher, M. Neubert and L. L. Yang, Eur. Phys. J. C **62** (2009) 333 [arXiv:0809.4283 [hep-ph]].

[28] C. Anastasiou, R. Boughezal and F. Petriello, JHEP **0904** (2009) 003 [arXiv:0811.3458 [hep-ph]].

[29] D. de Florian and M. Grazzini, Phys. Lett. B **674** (2009) 291, arXiv:0901.2427 [hep-ph].

[30] C. Anastasiou, S. Buehler, F. Herzog and A. Lazopoulos, arXiv:1107.0683 [hep-ph].

[31] A. Djouadi, Phys. Rept. **457** (2008) 1 [arXiv:hep-ph/0503172].

[32] S. Dittmaier *et al.* [LHC Higgs Cross Section Working Group], arXiv:1101.0593 [hep-ph].

[33] R. V. Harlander, F. Hofmann and H. Mantler, JHEP **1102** (2011) 055 [arXiv:1012.3361 [hep-ph]].

[34] G. Degrassi, S. Di Vita and P. Slavich, arXiv:1107.0914 [hep-ph].

[35] V. A. Smirnov, "Applied asymptotic expansions in momenta and masses," Springer Tracts Mod. Phys. **177** (2002) 1.

[36] S. A. Larin, Phys. Lett. B **303** (1993) 113 [arXiv:hep-ph/9302240].

[37] A. Pak, M. Rogal and M. Steinhauser, Phys. Lett. B **679** (2009) 473 [arXiv:0907.2998 [hep-ph]].

[38] K. G. Chetyrkin, B. A. Kniehl, M. Steinhauser and W. A. Bardeen, Nucl. Phys. B **535** (1998) 3 [arXiv:hep-ph/9807241].

[39] P. Nogueira, J. Comput. Phys. **105** (1993) 279.

[40] R. Harlander, T. Seidensticker and M. Steinhauser, Phys. Lett. B **426** (1998) 125, arXiv:hep-ph/9712228.

[41] T. Seidensticker, arXiv:hep-ph/9905298.

[42] S. Laporta and E. Remiddi, Phys. Lett. B **379** (1996) 283, arXiv:hep-ph/9602417.

[43] S. Laporta, Int. J. Mod. Phys. A **15** (2000) 5087, arXiv:hep-ph/0102033.

[44] A. D. Martin, W. J. Stirling, R. S. Thorne and G. Watt, Eur. Phys. J. C **63** (2009) 189 [arXiv:0901.0002 [hep-ph]].

[45] M. Spira, arXiv:hep-ph/9510347.

[46] `http://www-ttp.particle.uni-karlsruhe.de/Progdata/ttp11/ttp11-21/`

[47] J. Blumlein and S. Kurth, Phys. Rev. D **60** (1999) 014018 [arXiv:hep-ph/9810241].

[48] D. Maitre, Comput. Phys. Commun. **174** (2006) 222 [arXiv:hep-ph/0507152].

[49] J. Ablinger, J. Blumlein and C. Schneider, arXiv:1105.6063 [math-ph].